Chapter 7: Advanced Lithium Metal Battery: Enhancing Electrochemical Performance with 3D-Printed Hierarchically Porous Copper Collectors

This chapter presents a comprehensive investigation into the characteristics and performance of LMBs, with a primary focus on their electrochemical behavior and structural properties. The study involves detailed morphological characterization of lithium deposition within a 3D-printed porous copper current collector, carried out under varying current densities and plating capacities to examine how these parameters influence deposition patterns.

The Coulombic efficiency of the system is evaluated at multiple current densities to assess the effectiveness of lithium plating and stripping processes, offering insights into the battery's energy efficiency and cycling stability. Electrochemical impedance spectroscopy (EIS) is employed to analyze the charge transfer resistance associated with the porous Cu current collector, enabling a deeper understanding of interfacial electrochemical behavior.

A comparative analysis is conducted between the 3D-printed porous copper current collector and conventional copper foil to highlight differences in lithium deposition behavior, charge transfer resistance, and overall electrochemical performance. In addition, XRD analysis is performed to investigate the crystalline structure and composition of lithium deposits formed on both types of current collectors, providing insights into the uniformity and phase characteristics of the deposits.

Through these investigations, the chapter aims to identify the key factors governing the behavior and efficiency of LMBs, with a particular emphasis on the influence of current

collector design on lithium deposition, impedance characteristics, and overall battery performance.

7.1 Results and Discussion

7.1.1 Fabrication of coin cell

A thin Cu electrode sample with a diameter of 16 mm, a thickness of 200 μm, and a designed pore size of 150 μm was developed specifically for LMBs. The sample was fabricated using optimized processing parameters derived from DIW analysis. Fig. 7.1 illustrates the successful fabrication of the complex-shaped, HP-Cu current collector using this methodology. Analysis revealed that the fabricated sample achieved a controlled pore size of 154 ± 10 μm. From Fig. 7.1(c), it is evident that all the Cu particles in the ink were fully wetted by the binder solution. Additionally, in the 3D-printed Cu green samples, the Cu particles were properly interconnected and uniformly surrounded by the binder. Following the sintering process, randomly distributed pores were observed within the 3D-printed high-particle-loading copper (HP-Cu) current collector. These pores, formed due to partial particle fusion and localized densification, act as favorable nucleation sites for lithium deposition during the charging cycle. By providing multiple, well-dispersed sites for lithium nucleation, the porous structure enables a more uniform distribution of lithium across the current collector surface. This uniformity helps to minimize localized lithium buildup, thereby significantly reducing the risk of dendrite formation. Additionally, the pores help accommodate volume changes during cycling, contributing to improved

structural stability and longer cycle life of the lithium metal battery.

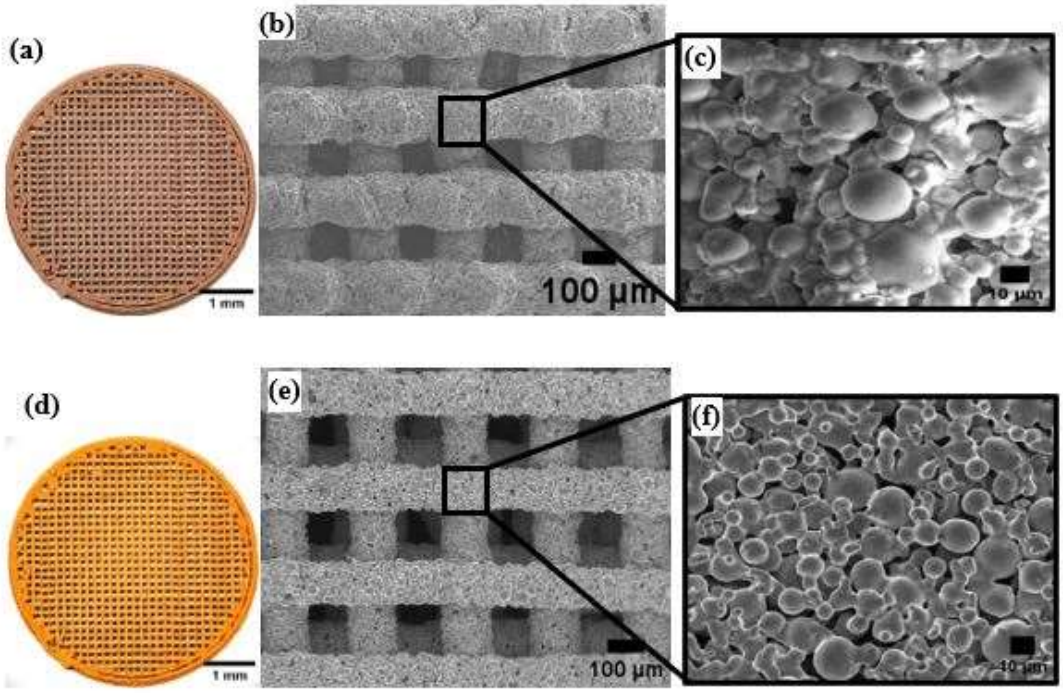

Fig. 7.1: -(a) Green sample (b-c) SEM of the green sample (d) Sintered sample of the (e-f) SEM after debinding and sintering of HP-Cu current collector

7.1.2 Electrochemical performance

Discharge profiles in LMB provide critical information about the electrochemical performance, stability, and capacity of the system. When comparing flat Cu foil and HP-Cu as current collectors, the discharge profiles reveal significant differences due to their structural and electrochemical properties. The discharge profile of the Cu foil shown in Fig. 7.2 indicates that there was sudden voltage drop with significant voltage fluctuations and unstable plateau after several cycles. This behavior was attributed to non-uniform lithium deposition and the growth of dendrites, which caused localized fluctuations in voltage due to uneven current distribution. [118]. Moreover, repeated cycle causes cracks, increasing resistance and instability in the discharge profile. The localized voltage drop sometimes causes internal short circuit and capacity fade. Moreover, for the HP-Cu current collector,

discharge profiles show a stable and flat voltage plateau over multiple cycles. The voltage drop is gradual, even after extended cycling, and overall capacity remains higher than that of flat Cu. Fig. 7.2 shows the nucleation overpotential in Cu foil and the HP-Cu current collector.

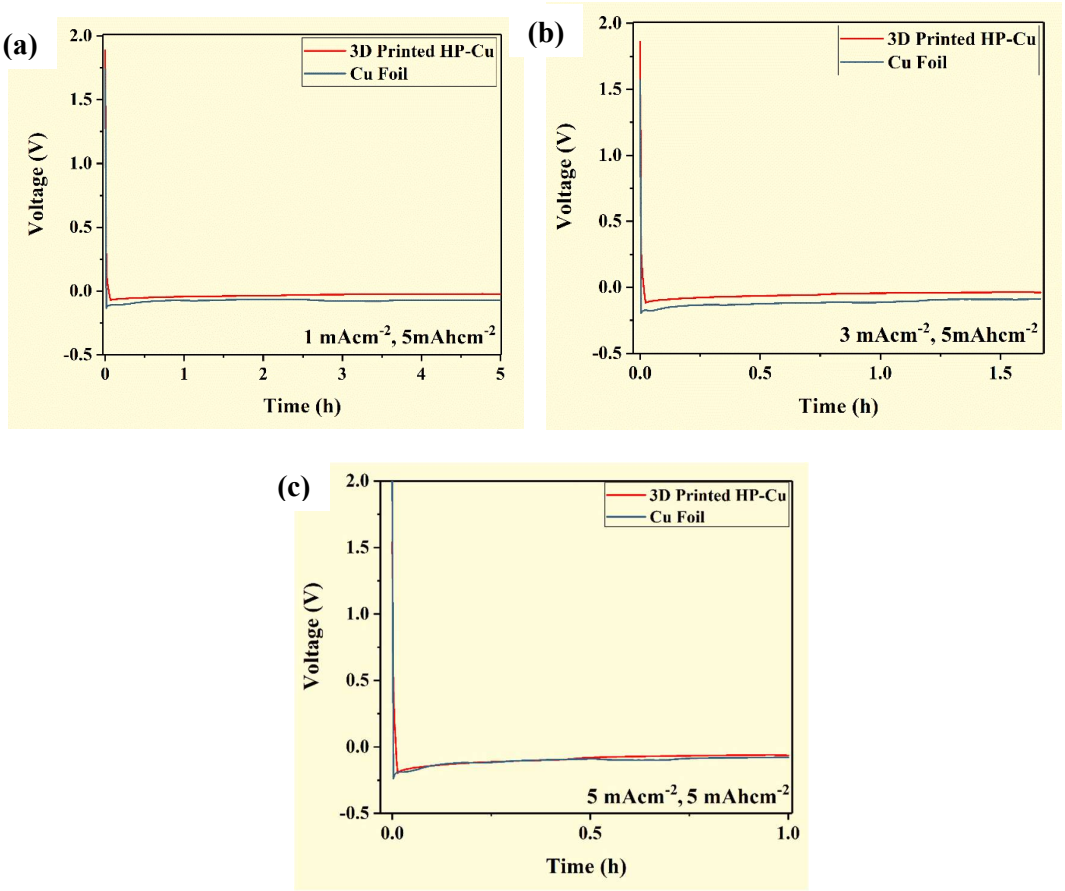

Fig. 7.2: Discharge profile of Li plating at current density of a) 1 $\mathrm{mAcm^{-2}}$,b) 3 $\mathrm{mAcm^{-2}}$ and (c) 5 $\mathrm{mAcm^{-2}}$ at a plated capacity of 5 $\mathrm{mAhcm^{-2}}$

The nucleation overpotential in the discharge profile reflects the energy barrier for lithium nucleation and growth during deposition. As seen in Fig. 7.2, it appears at a more negative voltage for the Cu foil compared to the HP-Cu current collector, indicating more favorable nucleation conditions on the porous HP-Cu surface. This can be attributed to differences in electrochemical behavior and structural properties of the two materials.

Cu foil has fewer nucleation sites and a smoother surface, requiring a higher overpotential (lower voltage) to overcome the energy barrier for Li nucleation. This leads to the nucleation overpotential appearing at a lower voltage, reflecting the energy required to start the Li plating process. Since current density is inversely proportional to surface area, high local current density increases overpotential, contributing to the nucleation overpotential in the discharge profile. Cu foil has a smaller effective surface area, leading to higher local current densities during Li deposition. This amplifies the overpotential required for plating, shifting the nucleation overpotential to lower voltages. Another reason for the negative nucleation overpotential formation was attributed to limited surface accessibility and uniformity resulting in poor Li-ion transport to active deposition sites. This increases the transport resistance, requiring a larger driving force (lower voltage) for Li deposition, shifting the nucleation overpotential downward. Li tends to deposit as isolated islands initially, which requires overcoming a significant nucleation barrier, reflected in the nucleation overpotential at a lower voltage. Whereas the HP-Cu provides numerous nucleation sites, reducing the energy barrier for Li deposition. As a result, the nucleation overpotential occurs at a less negative voltage since Li nucleation starts more easily and uniformly. The high surface area of the porous structure lowers the local current density, reducing the overpotential and causing the nucleation overpotential to appear at a higher voltage. Moreover, porous structure allows efficient ion transport to the deposition sites, minimizing resistance and shifting the nucleation overpotential to a less negative voltage. Another reason for the upward nucleation overpotential formation in comparison to Cu foil is that Li deposition is confined within the pores, maintaining a uniform energy distribution and reducing the magnitude and position of the nucleation overpotential.

Moreover, it can also be observed from the Fig. 7.2 (b-c) that as the value of current density increases the nucleation overpotential formation slightly shifts towards negative potential.

When the current density of the charge-discharge cycle increases, the nucleation overpotential shifts to lower (more negative) potential. Since at higher current densities, the local current at the electrode-electrolyte interface increases, leading to greater resistance and battery requires a higher overpotential to drive the Li deposition process, shifting the nucleation overpotential to lower potential. Moreover, Li nucleation becomes more difficult at higher current densities due to increased competition for deposition sites and higher current density amplifies the energy barrier for forming stable nuclei, requiring a more negative voltage to overcome this barrier and initiate the plating process. Hence, based on the above discussion it could be inferred that the nucleation overpotential in the discharge profile appears at a lower (more negative) voltage for flat Cu foil because of higher nucleation overpotentials, poor current distribution, and higher Li-ion transport resistance. In contrast, HP-Cu reduces these effects through its high surface area, uniform Li deposition, resulting in the nucleation overpotential occurring at a less negative voltage. These properties make 3D printed HP-Cu more efficient in facilitating smoother Li deposition and reducing energy loss.

Moreover, for checking the performance of the 3D-printed HP-Cu electrode for EES applications, the prepared sample has been used in LMBs system. The efficiency of the sample was measured and compared with 3D-printed planar Cu coin to evaluate its efficacy. It can be observed from Fig. 7.3 (a) that 3D-printed HP-Cu current collector exhibited the highest coulombic efficiency of 95.86% for more than 400 h. It can also be inferred from Fig. 7.3 (a) that 3D-printed HP-Cu current collector showed a stable cycle with limited fluctuation. This could be attributed to prevention of the dendrite formation at the anode side of the battery. The study highlighted a significant difference in the performance of 3D-printed planar Cu coins and 3D printed HP-Cu structures in the context of electrochemical energy storage applications. Notably, the coulombic efficiency of the 3D-printed planar Cu

coin was determined to be 75.48%. However, this efficiency experienced a substantial decline at a rapid pace, particularly after 150 h of operation. The relatively poor coulombic efficiency observed in the planar Cu coin can be attributed to the formation of dendritic structures. These dendrites are a common issue in battery systems and are known to cause detrimental effects, such as short-circuiting, which compromises the overall stability and functionality of the battery system .

Furthermore, the study investigated the performance of the two types of current collectors under varying current densities, specifically analyzing their behavior when the current density was increased from 1 mA cm^{-2} to 3 mA cm^{-2}. The results revealed a marked improvement in the stability and performance of the 3D-printed HP-Cu current collector compared to the 3D-printed planar Cu coin. Under these conditions, the HP-Cu structure demonstrated exceptional stability, maintaining its structural and electrochemical integrity even after 150 h of operation. In stark contrast, the planar Cu coin exhibited a significant loss of stability, becoming unreliable after only 40 h of operation at a current density of 3 mA cm^{-2}.

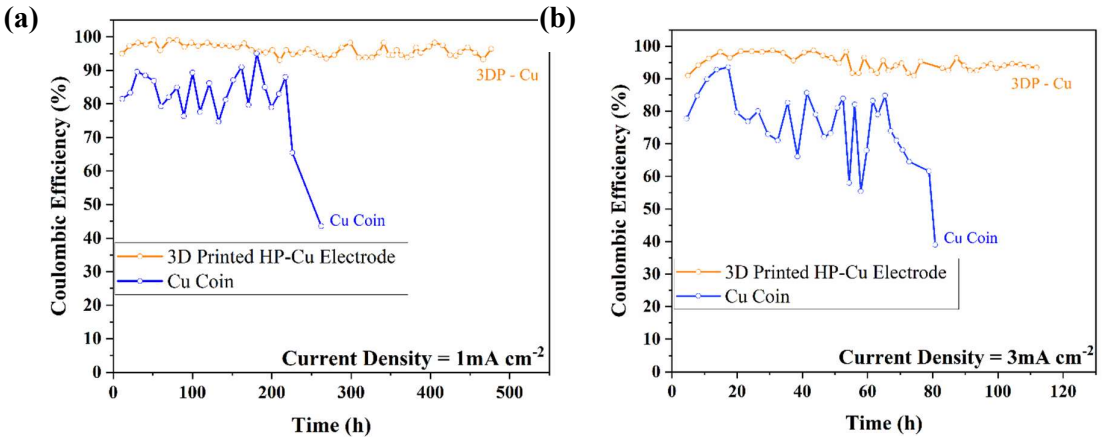

Fig. 7.3: Comparison of Coulombic efficiency of 3D printed HP-Cu current collector and 3D printed Cu coin at a) current density of 1 $mAcm^{-2}$ and b) current density of 3 $mAcm^{-2}$ at a plated capacity of 5 $mAhcm^{-2}$.

Fig. 7.4 compares the coulombic efficiency of a 3D-printed HP-Cu current collector with that of a conventional Cu foil. The 3D-printed HP-Cu current collector demonstrates a coulombic efficiency of 95.86 % over a 400 h, with minimal fluctuations throughout the cycles. In contrast, the Cu foil achieves a coulombic efficiency of only 66.34% and sustains cycling for just 250 h. The reason for the higher coulombic efficiency of the 3D printed HP-Cu current collector was the higher surface area compared to flat Cu foil which reduces the local current density, leading to more uniform Li deposition.

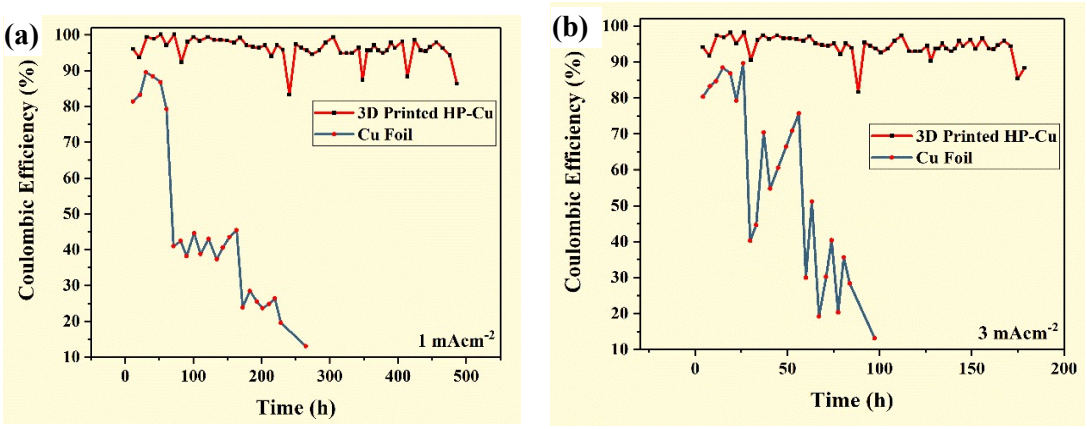

Fig. 7.4: Comparison of coulombic efficiency of 3D printed HP-Cu and the Cu foil at current density of (a) $1mAcm^{-2}$ and (b) $3mAcm^{-2}$ at capacity of 5 $mAhcm^{-2}$

Moreover, the porous structure facilitates controlled Li deposition within its framework, promoting the formation of a uniform and stable solid electrolyte interphase. The porous framework suppresses the initiation and growth of dendrites by guiding Li deposition into the structure rather than allowing protrusions to form outward. Due to which internal short circuits and capacity fade were prevented maintaining high coulombic efficiency. It can also be observed from the Fig. 7.4 (b) that as the current density increases, the 3D printed HP-Cu current collector still shows the stable cycle for more than 200 h whereas the coulombic efficiency of Cu foil drops suddenly, and it lasted only for less than 100 h. In contrast, the Cu foil fails prematurely (within 100 h) due to uneven deposition, and dendrite growth, which are exacerbated at higher current densities. Moreover, Cu foil has a flat

surface with limited nucleation sites for Li deposition leading to non-uniform Li deposition and the formation of dendrites. Uneven deposition causes localized overpotentials during subsequent cycles and disrupts the SEI, requiring frequent repair that consumes Li and electrolyte, causing variable efficiency across cycles. Hence the fabricated HP-Cu current collector shows better potential stability comparison to Cu foil.

7.1.3 Morphological Characterization

Fig. 7.5 (a-b) shows the deposition of the Li ion in the porous Cu electrode. It can be observed that Li-ion deposition in a porous Cu current collector occurs in a more uniform and controlled manner due to the structural and electrochemical advantages provided by the porous architecture.

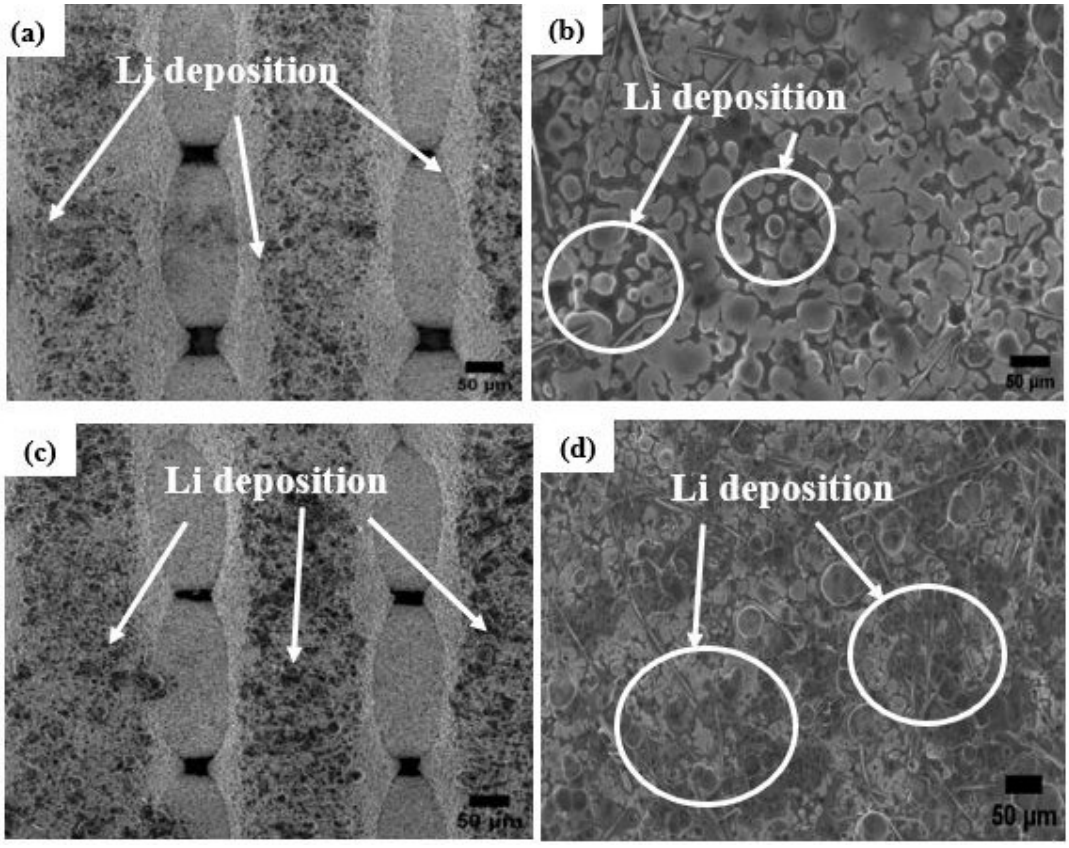

Fig. 7.5: shows SEM images of Lithium deposition at current density of 3 $mAcm^{-2}$ at a plated capacity of 5 $mAhcm^{-2}$ (a-b) After 10 cycles (c-d) After 20 cycles

Li ions in the electrolyte migrate to the electrode surface under the influence of the electric field. At the HP$-Cu$ current collector Li^+ions gain electrons e^- from the collector and are reduced to metallic Li^+. Metallic Li nucleates on the high-surface-area Cu framework and the porous structure provides numerous nucleation sites, reducing the likelihood of uneven deposition and dendritic growth. It can also be observed from the Fig. that during deposition Li fills the pores within the Cu structure. This allows Li to distribute throughout the porous network rather than building up a thick layer on the surface, preventing uneven plating.

Moreover, since porous structure promotes uniform deposition of Li that can be attributed to offer the higher active surface area, this lowers the effective current density reducing the risk of dendritic growth caused by localized high-current densities. In addition to this, as the number of cycles increases to 20 (Fig. 7.5 (c-d)), the Li ions are still uniformly deposited on the porous Cu current collector. gradual pore deformation and slight densification were observed, likely due to repeated lithium plating/stripping, which can stress the porous matrix over time. Additionally, localized thickening of the SEI layer may occur, increasing interfacial resistance. Despite these effects, no structural fracture was observed, and the electrode maintained a Coulombic efficiency above 95%, indicating strong mechanical stability and sustained electrochemical performance. Over time, this helps to maintain a more consistent and stable Li deposition process.

In comparison to traditional Cu foil, the porous structure of HP-Cu offers a significantly larger surface area and a more optimized pore structure. These characteristics contribute to its ability to effectively accommodate the Li volume expansion and facilitate a more uniform deposition pattern. This design feature is especially beneficial in preventing issues like dendrite formation and uneven plating, which can be problematic in conventional current collectors. As a result, the porous Cu current collector can sustain more consistent Li deposition, improving the overall performance and cycle life of the Li-ion battery.

Hence, the fabricated HP-Cu current collector enhances Li-ion deposition by providing a high-surface-area scaffold, ensuring uniform current distribution and Li growth. This architecture minimizes the risk of dendritic growth and improves the stability and safety of Li metal battery. Fig. 7.6 shows SEM images of Li deposition at current density of 1 $\mathrm{mAcm^{-2}}$ at a plated capacity of 5 $\mathrm{mAhcm^{-2}}$. It can be inferred from the Fig. 7.6 that Li metal starts filling pores of the porous Cu current collector after $200\,h$. As the time progressed i.e. after $400\,h$ all the pores were filled by Li ions. Even after $400\,h$, the pores were filled completely with Li without dendrite formation because the porous structure inherently ensures controlled and uniform Li deposition. The deposition starts with the inner surfaces of the pores and progresses outward as the Li gradually fills the voids, once all the pores are filled, Li deposition stops due to the lack of additional surface area within the porous network.

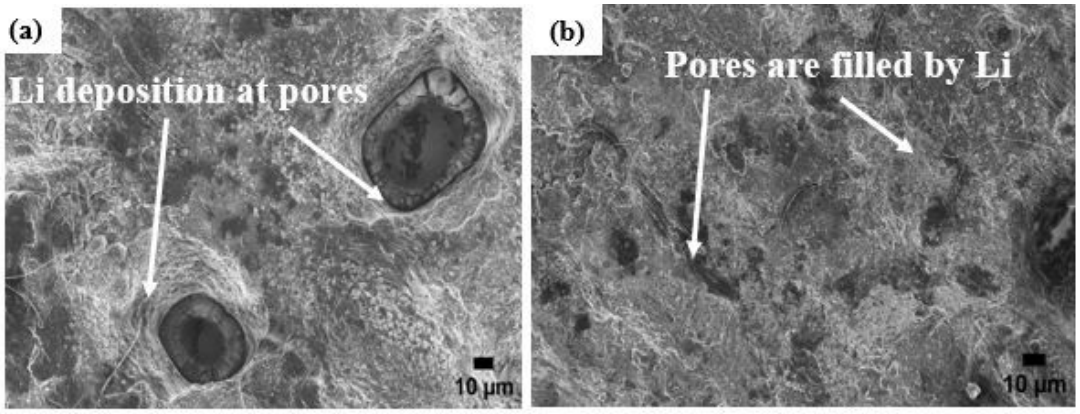

Fig. 7.6: SEM images of Li deposition at current density of 1 $\mathrm{mAcm^{-2}}$ at a plated capacity of 5 $\mathrm{mAhcm^{-2}}$ (a) After 200 h (b)After 400 h

It can also be inferred from Fig. 7.6 that the porous architecture accommodates the volume expansion of Li during deposition and contraction during stripping. Li grows within the pores, avoiding external stress on the electrode structure. Fig. 7.7 shows the Backscattered electron (BSE) imaging in a SEM provides critical insights into the morphology,

distribution, and uniformity of Li deposition in HP-Cu current collectors. Backscattered electrons originate from the elastic scattering of primary electrons off the sample.

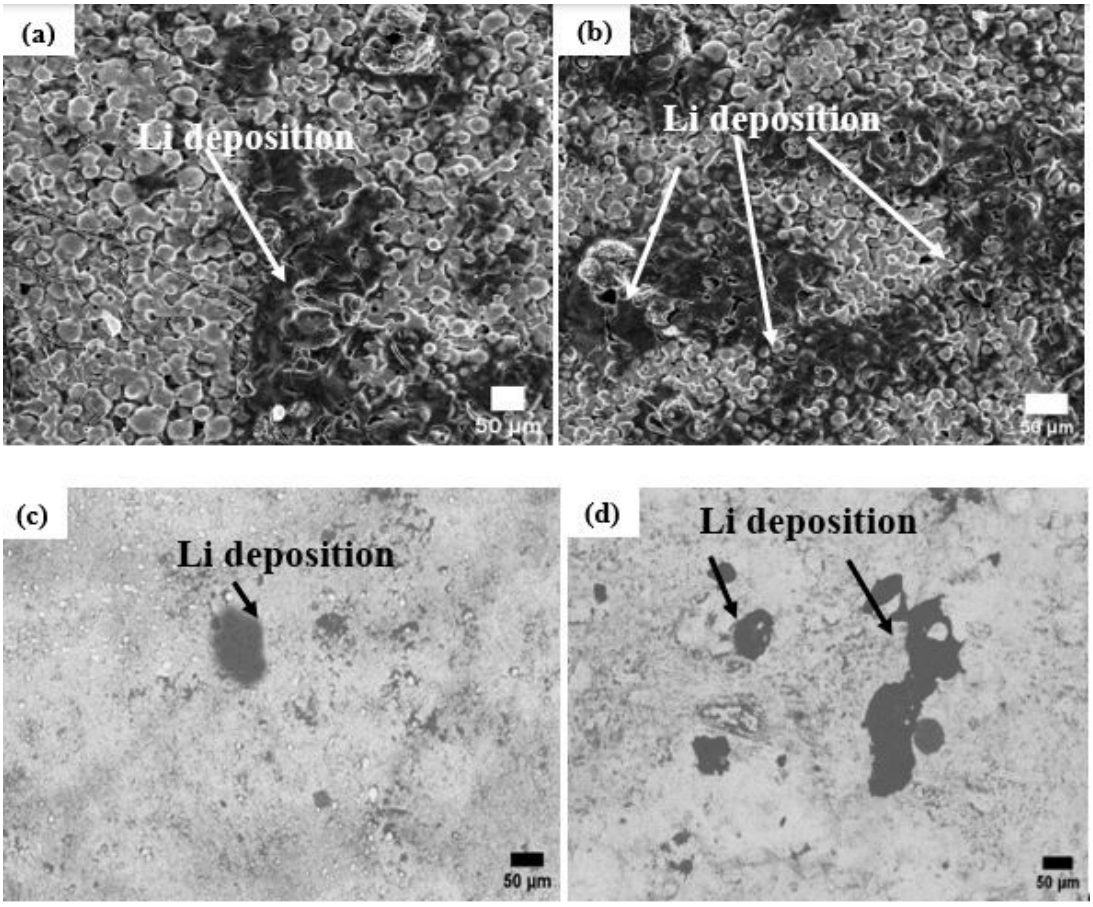

Fig. 7.7: BSE images of Li deposition at current density of (a-c) 1 $mAcm^{-2}$ (b-d) 3 $mAcm^{-2}$plated capacity of 5 $mAhcm^{-2}$ (a-b) porous HP-Cu (c-d) Cu foil.

Materials with higher atomic numbers (Z) produce more backscattered electrons and appear brighter in the images. Li with low value of atomic number appear darker, while Cu with high value of atomic number appears brighter. BSE images show bright Cu regions with small, scattered dark spots representing Li nucleation and dark spots are distributed uniformly within the pores of the Cu. Li deposition begins uniformly across the porous structure, with nucleation sites forming in the high-surface-area regions of the Cu and minimal growth outside the pores indicates that the deposition process is well-confined.

It can also be observed from the Fig. 7.7 that as the value of current density increases, the dark regions (Li) grow and increasingly fill the pores. However, the dark patches remain confined within the porous structure, and the overall brightness of the Cu framework is maintained. Also, Li deposition progresses layer by layer, with the porous Cu acting as a scaffold to direct and accommodate the growth. The void spaces within the pores get filled gradually with Li, maintaining uniform deposition and avoiding protrusions.

When the value of current density is increased to 3 $\mathrm{mAcm^{-2}}$ the pores are observed to be almost entirely filled with dark regions, representing fully deposited Li and the surface of the Cu remains smooth, with no protruding features or dendritic structures. Li fills the pores completely, forming a compact and uniform layer within the structure and the absence of bright or irregular features at the pore edges suggests no Li deposition outside the pores or dendrite formation. No sharp or protruding features (indicative of dendrites) are visible in the images, highlighting the ability of the porous architecture to confine Li growth. Figs. 7.7 (c) and (d) show the BSE images of Li deposition in Cu foil. The Cu foil appears bright with scattered, small, dark spots indicating initial Li nucleation sites. The appearance of small, dark nucleation sites reveals the preferential locations for Li deposition. These spots are randomly distributed or concentrated near the surface irregularities. Non-uniform darkening or clustering suggests uneven deposition, which can lead to dendrite formation and Li deposition starts at nucleation sites on the Cu surface and non-uniform distribution suggests higher local current densities or surface defects, which act as preferential sites for Li plating. After a few cycles dark regions expand and begin to form clusters, covering larger areas of the Cu surface. Some darker protrusions (indicating Li growth) may start appearing. Li deposition becomes more significant, with uneven growth leading to

clustering. This indicates a tendency toward irregular deposition, possibly the early stages of dendrite formation if local overpotentials are not well-controlled.

It can be observed from the Fig. 7.7 (d) that Li forms thicker layers, with uneven growth patterns indicating non-uniform current distribution and protrusions or dendrites are likely forming due to high local current densities and uneven Li -ion flux. The main reason behind the formation of dendrites and non-uniform deposition of Li was a limited surface area, which leads to higher local current densities. Moreover, surface defects or roughness on flat Cu foil serve as preferential nucleation sites, causing uneven Li deposition. Hence unlike 3D Printed HP-Cu, flat Cu does not physically confine Li growth, making it more prone to forming protrusions and dendrites.

7.1.4 XRD Analysis

Figures 7.8 (a-c) show the XRD patterns of as-sintered porous Cu, Li deposited Cu foil after 10 cycles and Li deposited 3D printed HP-Cu after 10 cycles, respectively. From the Fig. 7.8 (a) it could be seen that the sintered Cu sample exhibits peaks related to Cu only, thereby indicating that the sample was free from oxygen. It can be observed from the Fig. 7.8 that the peaks correspond to pure Cu were at 2Θ angle of 43.3°, 50.4°, 74.1° in HP-Cu, Cu foil and Li deposited porous Cu. A reduced Cu peak intensity at an angle of 74.1° could be observed Fig. 7.8 (c) as compared to Figs. 7.8 (a and b) which may be attributed to the deposition of Li on the surface of Cu. In place of Li, Li hydroxide was formed due to reaction with the moisture after disassembly. It can also be observed from the Fig. 7.8 that all the other peaks except at 2Θ angle of 43.3°, 50.4°, 74.1° were the peaks of Li hydroxide.

The presence of distinct peaks in the XRD patterns clearly confirms the successful deposition of lithium metal on both the conventional Cu foil and the hierarchically porous copper (HP-Cu) current collector. A closer examination of Fig. 7.8 reveals a notable

difference in peak intensity between the two substrates. The peaks associated with Li on the Cu foil exhibit significantly higher intensities. This can be attributed to the dense, non-porous nature of the Cu foil, which presents a relatively smooth and compact surface. In such a configuration, Li metal tends to deposit uniformly across the surface, forming larger and more coherent crystalline domains. These well-aligned crystallites contribute to sharper and more intense diffraction peaks.

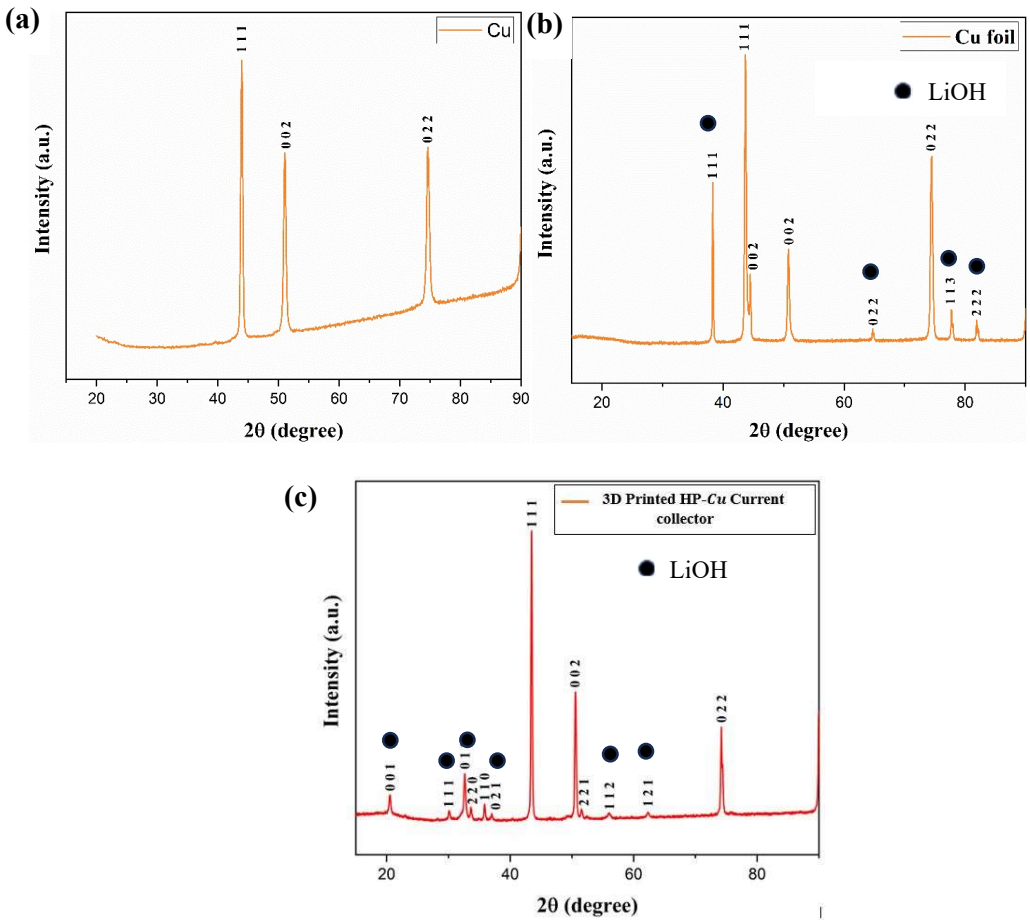

Fig. 7.8: XRD pattern of (a) As-sintered porous Cu; (b) Li deposited Cu foil after 10 cycles and (c) Li deposited 3D printed HP-Cu after 10 cycles

In contrast, the XRD pattern of the HP-Cu current collector displays comparatively weaker and less intense Li-related peaks. This difference arises primarily due to the highly porous and complex architecture of the HP-Cu structure. In this case, Li deposition does not occur

only on a flat surface but is distributed over a much larger and more irregular surface area, including the internal walls of the pores. The increased surface roughness and heterogeneous topography of the HP-Cu lead to the formation of smaller, randomly oriented lithium crystallites. Additionally, the confinement within the pores may hinder the long-range order typically required for strong diffraction signals. As a result, the lithium domains formed on the HP-Cu are less coherent and more dispersed, which collectively contribute to the observed broadening and reduction in the intensity of the XRD peaks. Moreover, it can also be observed from the Fig. 7.8 that on Cu foil, the intense peaks of Li in XRD indicate highly crystalline regions, which can be associated with dendritic Li growth on flat Cu foil. These dendrites have a well-defined crystal structure, leading to sharp and intense XRD peaks. In porous Cu, smaller and broader Li peaks in the XRD pattern indicate a more uniform and dispersed deposition of Li. Cu reduces localized current density by distributing the electrochemical reactions across a larger surface area as Li deposits more evenly, often forming smaller crystallites or even amorphous layers, leading to weaker and broader peaks in the XRD pattern. This uniform deposition of Li on the porous Cu reduces the risk of dendritic growth, which lead to avoidance of short circuits and safety hazards in Li metal batteries. Uniform deposition minimizes stress and prevents dead Li formation during cycling whereas Intense Li peaks suggest large, crystalline Li deposits, which are often linked to dendritic structures. Hence, fabricated HP-Cu current collector is able to effectively prevent the dendrite growth, making it an attractive solution for enhancing performance and safety of Li metal batteries.

7.1.5 Impedance Analysis

Fig. 7.9 shows the equivalent circuit diagram and the impedance plot for the Cu foil and 3D printed HP-Cu after zero cycle and five cycles. In the equivalent circuit diagram, R_1 represents the electrolyte resistance, R_{SEI}, the SEI layer resistance while R_{CT} represents the

charge transfer resistance. W_s represents the Warburg impedance and C_{dl} the double layer capacitance. R_1 accounts for the ionic resistance of the electrolyte, the conductivity of the separator, and the electronic resistance of the current collector and its value depending on the electrolyte conductivity

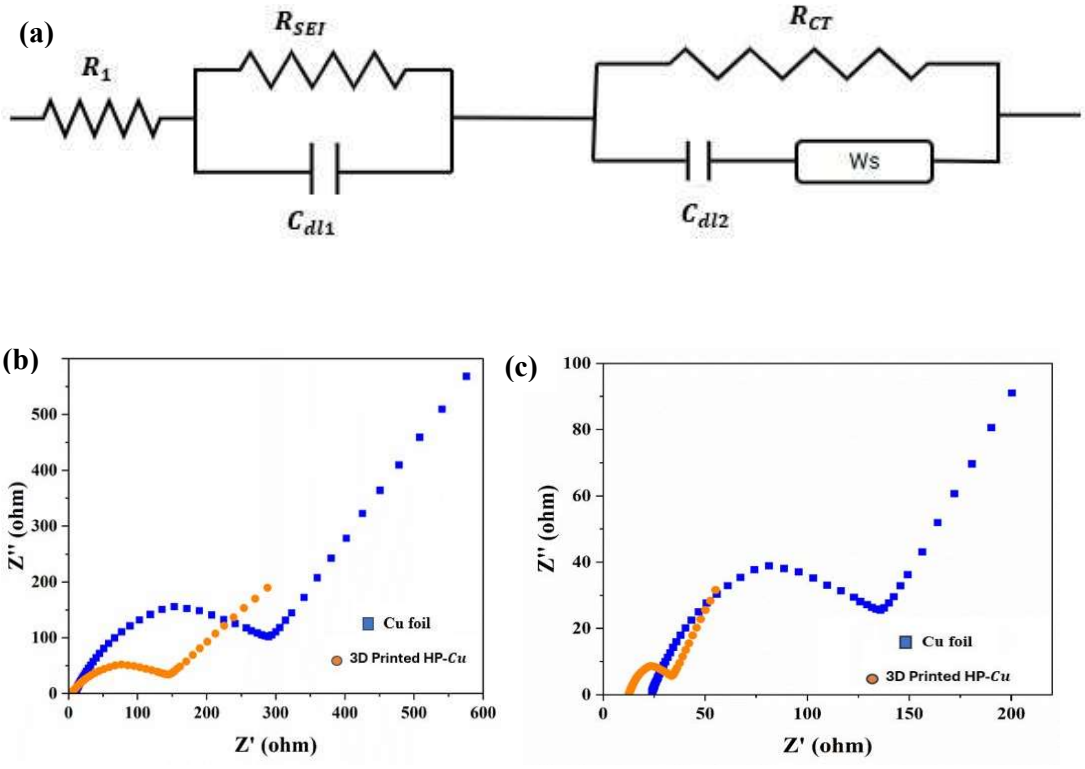

Fig. 7.9: (a) Impedance circuit diagram (b-c) Impedance plot for planar Cu foil and 3D printed Cu (b) zero cycle (c) After 5 cycles

. R_{SEI} represents the impedance associated with the SEI layer formed on the Cu foil due to Li plating. R_{CT} represented by the diameter of the main semicircle in the high-frequency range and indicates the resistance for the Li-ion intercalation reaction at the electrode/electrolyte interface. Its value is affected by the surface area of the Cu foil and electrode. Warburg impedance is straight line having slope of 45° and represents the diffusion of Li ions through the SEI layer, electrolyte, and active material. If the slope of the impedance in an EIS in Nyquist plot is a straight vertical line at 90°, it does not

represent Warburg impedance. Instead, it indicates pure capacitive behavior, a non-diffusion-controlled process. C_{dl} is called double-layer capacitance because it arises from the electrical double layer, which stores charge at the electrode/electrolyte interface in a manner analogous to a physical capacitor. Among the resistances discussed above charge transfer resistance is the most important parameter for the dendrite growth prevention and represents the resistance to the electrochemical reaction at the electrode-electrolyte interface, where Li ions are reduced to metallic Li during plating and oxidized during stripping. Charge transfer resistance acts as a kinetic barrier to the rate of Li-ion reduction at the electrode interface. If its value is too low, Li can deposit too rapidly, leading to uneven nucleation and the growth of dendrites. Hence, a balanced charge transfer resistance ensures controlled deposition, allowing Li to deposit in a smooth, dense layer.

Fitting the experimental data reveals that the apparent charge transfer resistance for the HP-Cu foil is 169 Ω, significantly lower than the 279.3 Ω observed for flat Cu foil. This finding suggests that the HP- Cu collector promotes the formation of a more stable SEI film at the electrode-electrolyte interface. Moreover, it can also be observed from Fig. 7.9 (b-c) that after five cycles, the charge transfer resistance of both cycles was reduced, however the value of the charge transfer resistance for the HP-Cu was lower than the Cu. The semicircle obtained in the Nyquist plot for the HP-Cu is flatter than the Cu foil resulting in flatter SEI. A flatter SEI layer implies that Li plating occurred more uniformly. Moreover, the semicircle obtained for the HP-Cu is smaller than the Cu foil which results in the low value of the R_{SEI}. This suggests a flatter, thinner, or more homogeneous SEI layer, facilitating easier ion transport and its lower value indicates that the SEI layer has fewer defects or is composed of materials with higher ionic conductivity. However, Cu foil might form a thicker SEI due to concentrated current density or surface imperfections. The semicircle size reflects the quality of the SEI layer. A smaller semicircle for the porous

Cu collector indicates a smaller SEI impedance and, consequently, a flatter SEI layer, which benefits Li plating and overall electrochemical performance.

This highlights the advantage of using HP-Cu for achieving more uniform and efficient electrochemical interfaces. It can also be observed that the real axis of the Nyquist plot denotes the resistance value while the y axis denotes the capacitance value. A smaller semicircle in the Nyquist plot for HP-Cu reflects lower charge transfer resistance. This characteristic enables uniform charge transfer and Li deposition, reduced current density and overpotential, enhanced SEI stability and ionic transport. These factors collectively suppress dendrite growth, making porous HP-Cu a superior current collector for Li -ion batteries. Whereas Cu foil has larger semicircle (high charge transfer resistance), larger semicircle can cause uneven reaction kinetics, leading to localized overpotentials that accelerate Li deposition in specific regions. Hence, fabricated HP-Cu current collector exhibits a superior impedance profile compared to traditional Cu foil in LMB.

7.1.6 Comparison study

Table 7.1 represents the comprehensive comparison of electrochemical performance of HP-Cu current collectors fabricated using manufacturing technique and having different pore morphology. The purpose of this study is to evaluate the efficacy of the present work in energy storage. It could be inferred from Table 7.1 that the 3D printed HP-Cu sample fabricated in the present work exhibited satisfactory electrochemical performance as compared to similar studies. It can be observed from the table that, It can be observed from the Table 7.1, that more costly or complex binders such as polyvinylidene fluoride (PVDF) used by Chen et al. [119], and Pluronic F-127 (PF127) used by Lim et al. [120].

Table 7.1 Comparison of Porous electrodes for LMB fabricated by various techniques

S No.	Author	Anode Material	Fabrication Method	Pore size (µm)	Nature of pore	Coulombic Efficiency (%)	Current density ($mAcm^{-2}$)	Capacity ($mAhcm^{-2}$)	Electrolyte
Present Study		Cu	DIW using PLA as a binder	154 ± 10 µm	Ordered	more than 95 % and steady after 400 h	1	5	1 M LiTFSI in DOL/DME (v/v 1:1) with 1.0 wt% LiNO3
1.	Callegari et al. [82]	Cu	DIW using PF-127 as binder	-	Patterned structures	Higher than 95 % after for 300 h	2	2	1 M lithium bis(fluorosulfonyl)imide (LiFSI) in EC:DMC (50 : 50 vol.%)
2	Chen et.al [119]	Cu	DIW using Poly (vinylidene fluoride) (PVDF) as binder	400 µm	Ordered	More than 98 % after 500 cycles	1	1	1 M LiTFSI DOL/DME (1:1) with 1 wt% $LiNO_3$
3	Lim et.al [120]	Cu	DIW using Pluronic F127 (PF127) as binder	300 µm	Ordered	More than 95 % after ~63 cycles	1	5	1 M LiTFSI DOL/DME (1:1) with 1 wt% $LiNO_3$
3	Qiu et.al [22]	Cu	Hydrogen Bubble	24-80 µm	Ordered	≈ 97 % after 150 cycles	0.5	1	1 M LiTFSI DOL/DME

			Dynamic Template						(1:1) with 1 wt% $LiNO_3$
4	Li et.al [121]	Cu	Electrodepositio n	60-170 µm	Ordered	≈ 94 % after 100 cycles	0.5	1	1 M LiTFSI DOL/DME (1:1) with 1 wt% $LiNO_3$
4	Zhang et.al [122]	Cu	Electrochemical oxidation	2.9-89 µm	Random	≈ 98 after 100 cycles	0.5	1	1 M LiTFSI in DOL/DME (v/v 1:1) with 2.0 wt% LiNO3
5	Liu et.al [18]	Ni foam	Deposition-dealloying	100nm-1 µm	Random	≈95 after 350 cycles	1	1	1 M LiTFSI in DOL/DME (v/v 1:1) with 2.0 wt% LiNO3
6	An et.al [123]	Cu	Vacuum distillation	-	Random	Steady for 120 cycles	0.52	0.26	1.0 M LiPF6 in EC/DEC with 1% (v:v)
7	Ma et.al [124]	Cu	Electrodepositio n	-	Random	≈ 99 for 100 cycles	2	1	1 M LiTFSI DOL/DME (1:1) with 1 wt% $LiNO_3$
8	Wang et.al [125]	Cu	Lithiophilic interphase in vertical micro-channels	-	Random	Steady value over 100 cycles	3	3	1 M LiTFSI in DOL/DME (v/v 1:1) with

									2.0 wt% LiNO3-
9	Lu et.al [8]	Li-Cu alloy	Li was deposited in Cu foam	-	Random	No Dendrite formation after 100 cycles	1	1	1 M LiTFSI DOL/DME (1:1) with 1 wt% $LiNO_3$
10	Wang et.al [126]	Cu	Vertically aligned microchannels	15-45 µm	Random	≈ 98 % after 200 cycles	1	1	1 M LiTFSI DOL/DME (1:1) with 1 wt% $LiNO_3$
11	Yun et. al [127]	Cu	Dealloying	200 nm to 2 µm	Random	≈ 97% after 200 cycles	0.5	1	1 M LiTFSI DOL/DME (1:1) with 1 wt% $LiNO_3$
12	Zhao et.al [128]	Cu	Electrochemical Dealloying	1 µm	Random	≈98 after 200 cycles	1	1	1 M LiTFSI in DOL/DME (v/v ¼ 1:1)
13	Qin et.al [129]	Cu	Powder Metallurgy	-	Random	≈98 %after 140 cycles	0.5	1	1 M LiTFSI in DOL/DME (v/v 1:1) with 2.0 wt% LiNO3-

The random and less controlled pore morphologies typically observed in alternative methods such as electrodeposition (Li et al.) [121], hydrogen bubble templating (Qiu et al.) [22], and dealloying (Yun et al.) [127]. Chen et al. [119] and Qiu et al. [22] reported slightly higher CEs of 98% and 97%, respectively, their results were achieved at significantly lower capacities (1 mAh/cm²). Notably, Liu et al.[18], who tested a SnCu scaffold under similar high-capacity conditions (5 mAh/cm²), reported a lower CE of 94.2%, highlighting the superior electrochemical stability achieved in the present work.

In this study, a novel, cost-effective, and environmentally sustainable approach has been developed for the fabrication of hierarchically porous copper (HP-Cu) current collectors using Direct Ink Writing (DIW). The method utilizes a high particle-loaded copper ink formulated with polylactic acid (PLA), a biodegradable and affordable binder, offering a significant improvement over conventional strategies that rely on expensive and environmentally harmful binders such as polyvinylidene fluoride (PVDF) or Pluronic F127. By capitalizing on the biodegradability, low cost, and ease of processing of PLA, this work effectively addresses key challenges related to the sustainability and scalability of current collector manufacturing.

Electrochemical testing of the fabricated electrodes revealed a high Coulombic efficiency exceeding 95%, maintained consistently over 400 hours at a current density of 1 mA/cm² and a plating capacity of 5 mAh/cm². These results demonstrate not only excellent initial performance but also remarkable long-term cycling stability. Unlike previous approaches that often exhibit irregular porosity or limited durability, the proposed method achieves precise pore size control, strong mechanical integrity, and sustained electrochemical performance, highlighting its potential for next-generation lithium metal battery applications.

Overall, this work establishes a promising and scalable route for producing high-performance, copper-based current collectors tailored for lithium metal battery applications. By combining sustainable materials, advanced additive manufacturing techniques, and optimized microstructural design, it offers a compelling alternative to conventional methods—balancing performance, reproducibility, and environmental responsibility.